Table 1. Patient characteristics

Pt. no	T-stage		Location	COM movement (cm) (PE-PI)	GTV volume ratio (Tn/T50) Ungated treatement	Gated treatement
1	T4NOMO	3	pancreas body	1.0	0.92-1.04	0.95-1.04
2	T4N2MO	3	pancreas tail	0.6	0.94-1.27	1.00-1.05
3	T4NOMO	3	pancreas body-tail	0.4	0.88-1.00	0.90-1.00
4	T4NOMO	3	pancreas head	1.7	0.94-1.03	0.94-1.00
5	T4NOMO	3	pancreas head	1.2	0.93-1.00	0.94-1.00
6	T4NOMO	3	pancreas head	0.8	0.89-1.04	1.00-1.04
7	T4NOMO	3	pancreas head	0.7	0.85-1.00	0.89-1.00
Average				0.9	0.9-1.1	0.9-1.0

Abbreviations: ADC = adenocarcinoma; COM = center of mass; PE = peak exhalation; PI = peak inhalation; GTV = gross tumor volume; T50 = peak exhalation; Tn = respiratory phase.

When gas is not present in the bowel, the abdominal region is filled with tissue of almost uniform density. Here, WEL variation due to respiratory motion may be less problematic than in the lung region, where lung tumors are surrounded by low-density tissue. Against this, however, tumors in the abdominal region occur more closely to organs at risk (OARs) than do those in the thoracic region. Dosimetric comparison of the two treatment strategies is therefore clinically relevant in both charged particle and photon beam therapy.

Current treatment planning systems remain three-dimension based but optimize treatment parameters for a single respiratory phase only. Because thoracic and abdominal treatments are performed under free-breathing conditions, however, comparison of strategies throughout the treatment course should include information on respiratory phase, in other words the fully complete 4D dose calculation, including deformable registration (21–26). This is particularly important because radiation oncologists and medical physicists more easily understand the results of single-dose assessment (accumulated dose), including time information, than results for several dose assessments conducted at discrete respiratory phases.

Here, to compare respiratory-gated and respiratory-ungated treatment strategies using 4DCT datasets, we evaluated 4D scattered carbon ion beam distribution in the pancreatic region.

METHODS AND MATERIALS

Patients

The participants in this study were 7 patients with pancreatic tumors randomly selected from inpatient pancreatic cancer patients (adenocarcinoma; mean age ± SD, 60.9 ± 5.8 y) at our hospital who were receiving carbon ion beam treatment with chemotherapy (Table 1). All gave informed consent to participate in the study, which was approved by the Institutional Review Board of the National Institute of Radiological Sciences.

Treatment planning

To evaluate the two treatment strategies in the pancreatic region, we performed 4D treatment planning using carbon ion beam. The 4D treatment planning with photon beam involves assessing geometric motion to cover the internal target volume (ITV) and defining a monitor unit value at the reference point (27). Given the finite range of carbon ion beam and other charged particle beams, 4D treatment planning with these beams should also consider induced WEL variations due to respiratory motion. In this section, we describe the 4D treatment planning process (imaging, target definition, bolus design, and dose calculation), including respiratory motion.

Four-dimensional CT imaging. To acquire volumetric CT data as a function of time, 4DCT scanning was done under free-breathing conditions using a rapidly rotating cone-beam CT (CBCT). To minimize anxiety that would perturb the stable breathing pattern (*e.g.*, respiratory cycle, baseline drifts), 4DCT scanning was done after a 10-minute rest in the supine position on the CT bed. The CBCT was an integrated two-dimensional wide cylindrical detector (256 slices) with high spatiotemporal resolution (28, 29). Inasmuch as the scan range of this equipment in the superior–inferior direction is about 12 cm in a single rotation, the patient bed was not moved during 4DCT scanning. Because the CT volume obtained in this study was not a composite of several breathing cycles, 4DCT resorting errors did not occur, and 4DCT image quality was not affected by irregular breathing. Patients were fixed on the patient bed with immobilization (body cast in supine position) in accordance with routine practice in our center. The respiratory signal was acquired using a respiratory sensing system consisting of a position-sensitive detector sensor and infrared-emitting light marker (Toyonaka Kenkyujo, Osaka, Japan) (18) affixed to the patient's abdomen. Scan conditions were slice collimation of 128 × 1.0 mm, 0.5 sec in a single rotation, and scan time of less than 6 sec to obtain one respiratory cycle.

Volumes from the 4DCT datasets were classified into 10 phases (T0: peak inhalation, T50: peak exhalation) based on the amplitude of the respiratory signal. We chose an amplitude-based phase assignment method because of the greater accuracy of amplitude-based gated treatment over phase-based gating in clinical situations (30, 31).

Contouring. The gross tumor volume (GTV) and clinical target volume (CTV), which included the GTV plus a 5-mm margin and tumor encasement of the celiac trunk and/or superior mesenteric artery, pancreas, kidneys (right and left), and duodenum, were manually contoured on the CT data at peak exhalation (T50) by a certified oncologist (R.H. or T.Y.) with more than 10 years' clinical experience. All contours at other respiratory phases were then automatically calculated by B-Spline-based deformable registration (32). This registration calculates transformation maps based on the 4DCT data, which are then applied to the contours to transform

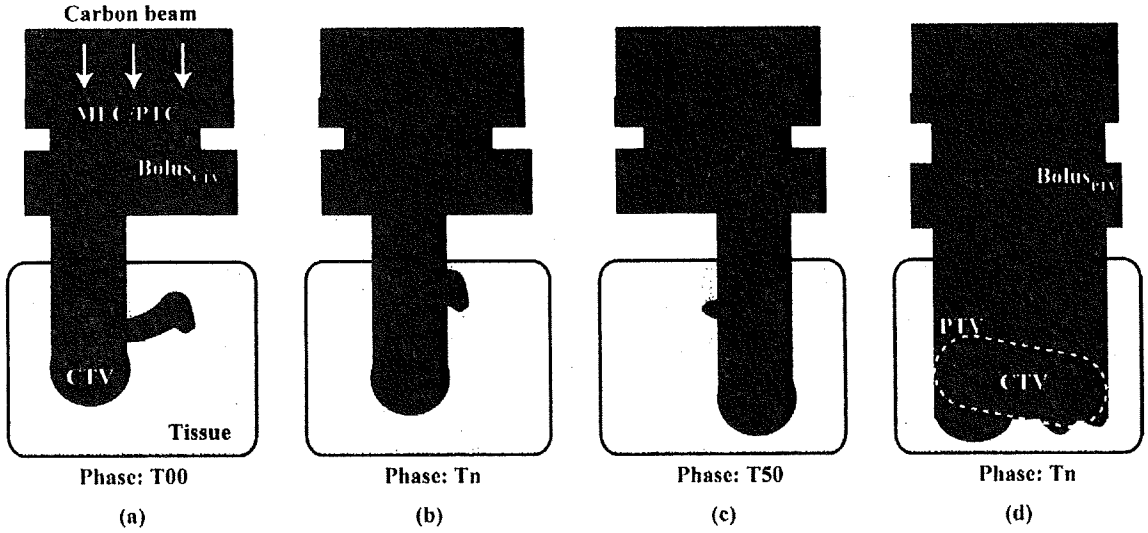

Fig. 1. Design bolus algorithm. (a) through (c) Compensating boli at respective phases were designed to stop the charged particle beam at the distal edge of the clinical target volume (CTV). (d) Boli for planning target volume (PTV) ($Bolus_{ungated}$, $Bolus_{gated}$) were calculated by selecting the maximum depth for $Bolus_{CTV}$ at the same position. Yellow dotted line shows the PTV region. MLC = multileaf collimator; PTC = patient collimator.

them from the peak exhalation phase to the other respiratory phases. Our registration accuracy test gave an approximate mean distance of 1.8 ± 0.3 mm (Table 1). The oncologist then checked the contour curves at each phase.

Two types of internal margin for the ungated and gated treatment strategies were calculated by combining respective CTVs to cover the whole and periexhalation CTV moving regions, which defined the 30% duty cycle around exhalation. A setup margin was not added because the same setup margin for ungated and gated treatment is not affected to investigate the difference between dose assessment for ungated and gated treatment. Planning target volumes ($PTV_{ungated}$ and PTV_{gated}) were calculated by adding the respective internal margin to the CTV at peak exhalation. This allowed the PTVs to encompass CTVs at respective phases.

Compensating bolus design. Two types of compensating bolus for the gated and ungated treatment were designed, as follows. First, boli ($Bolus_{Tn}$) for the CTV at the respective respiratory phases were calculated (Fig. 1a–c). The final compensating boli ($Bolus_{ungated}$ and $Bolus_{gated}$) were designed by selecting the minimum bolus thickness at the same position in the respective boli for a single respiratory cycle (10 phases) and around exhalation phases (T40–T60), respectively (Fig. 1d) to cover the PTV under each treatment strategy. The field boundary was defined using a patient collimator (PTC) or multileaf collimator (MLC). The PTC was used for field boundaries with a diameter less than 11 cm or to reduce excessive dose to an OAR near the target caused by the penumbra. margins of 3 mm and 6 mm for the PTC and MLC, respectively, were added outside the PTV to account for the penumbral effect. Additional smearing was not applied to the bolus, but consideration was given to smearing caused by physical construction with a 3-mm diameter drill, in accordance with our routine protocol.

Dose calculation and dose assessment. The carbon ion beam dose distribution was calculated as a function of respiratory phase by applying the compensating bolus to 4DCT at the respective phase. A total prescribed dose of 43.2 GyE (3.6 GyE/fraction) was delivered to the CTVs with four beam ports from 0°, 90°, 180°, and 270° because we used two paired fixed ports in the horizontal and vertical directions. In one of the patients (Patient 2), however, treatment was conducted from three beam angles (0°, 90°, and 180°) because the radiologic pathlength (range) from 270° (right side) to the distal edge of the target was shorter than the maximum range of the 400-MeV carbon ion beam. A beam angle of 0° was defined as the 12 o'clock position (standard International Electrotechnical commision [IEC] gantry angle notation) (33), with angles increasing clockwise. Beam energy for each beam field was selected from among 290 MeV, 350 MeV, and 400 MeV. The relative biological effectiveness (RBE) model used here is the same as our clinical routine (34). Dose calculation for each respiratory phase was performed with a pencil beam algorithm (35).

The accumulated dose distribution was calculated by registering the carbon ion beam distribution at the respective phases to that at peak exhalation (T50) by applying deformable registration, which creates transformation maps. The transformation maps were used to warp the contours from all other respiratory phases to peak exhalation. Dose values for each phase were accumulated on the basis of the respiratory signals for the duration of 4DCT imaging (respiratory weighting functions) (Fig. 2). Dose–volume histograms (DVHs) for GTV, CTV, kidney, pancreas, duodenum, and cord were calculated using the accumulated dose (4D-DVH).

All 4DCT data were transferred to a workstation and analyzed using the Aqualyzer system (2). This system calculates the 4D carbon beam dose distribution from measured carbon beam dose profile data and quantifies range variation as a function of time. All dose calculations were performed using the grid size of the original CT pixel size: 0.78 mm (anterior–posterior) × 0.78 mm (left–right) × 1.0 mm (superior–inferior).

RESULTS

Carbon ion beam dose distribution for ungated treatment as a function of respiratory phase is shown in Fig. 3 (Patient 1). Because the bolus was designed to cover the PTV and account for intrafractional respiratory motion, over 95% of the dose was delivered to the CTVs at all phases. Overdosing was caused by respiration-induced gas bowel positional changes (marked as arrows in Fig. 3). With gated treatment, beam field size on the inferior aspect was reduced, which in

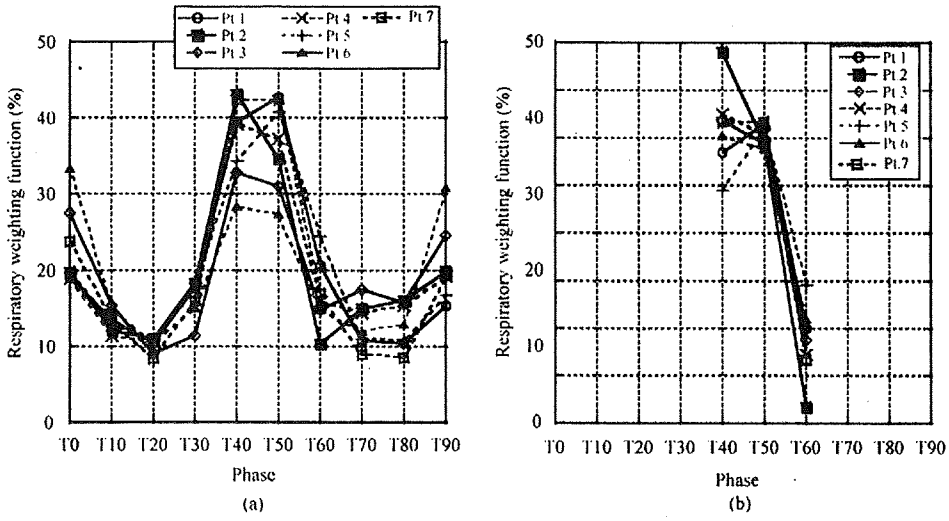

Fig. 2. Respiratory weighting function for (a) ungated and (b) gated treatments.

turn minimized excessive dosage to the normal tissues compared to that with ungated treatment (Fig. 4a b) (Patient 1).

To understand this result more clearly, we calculated the difference in accumulated dose distribution between the gated and ungated treatment by subtracting the accumulated dose distribution for the gated treatment from that for the ungated treatment (Fig. 4c). Large positive dose differences (over 10%) were observed mainly on the inferior aspect, resulting from the fact that gated treatment irradiates only during exhalation phases.

The DVHs for the ungated and gated treatments are summarized in Fig. 5a and b, respectively (Patient 1). Although DVH curves for the GTV, CTV, and cord did not change with respiratory phase, those for the duodenum and left kidney did. The 4D-DVH for the two treatment strategies is summarized in Fig. 5c. Because the bolus PTV was designed to cover CTVs at respective phases, D95 values for the GTV and CTV were greater than 97% of the prescribed dose for both strategies. For normal tissues, 4D-DVH curves were lower for the gated than the ungated treatment, albeit that the differences were small (Fig. 5c).

In another case (Patient 2), although tumor and normal tissues moved up and down with respiratory function, dose distribution varied less than in the previous patient (Patient 1) because the amount of bowel gas was low, tissues in the abdominal region are almost completely homogeneous, and beam weight was lower in the anterior–posterior direction than in the other directions (Fig. 6).

The DVHs for the ungated and gated treatments as a function of respiratory phase are summarized in Fig. 7a and b,

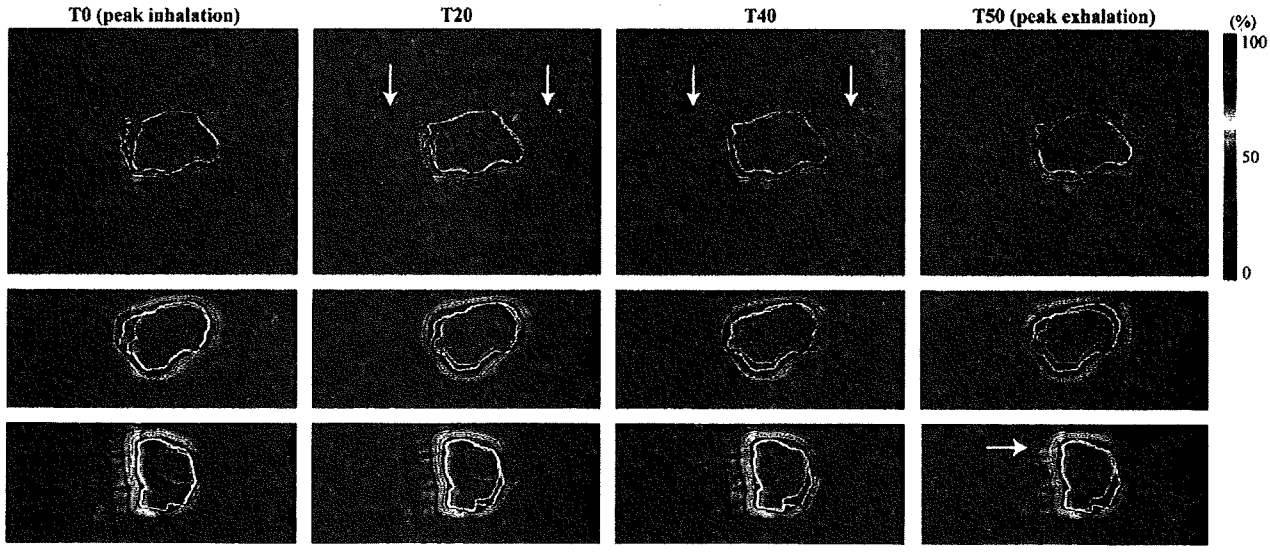

Fig. 3. Carbon ion beam dose distribution for ungated treatment (Patient 1). Axial (upper row), coronal (middle row), and sagittal (lower row) sections. White areas, yellow areas, and dark green lines show the planning target volume (PTV), clinical target volume (CTV), and gross tumor volume (GTV) contours, respectively. Red, green, pink, light blue, and blue lines show 95%, 80%, 70%, 50%, and 30% of total doses, respectively.

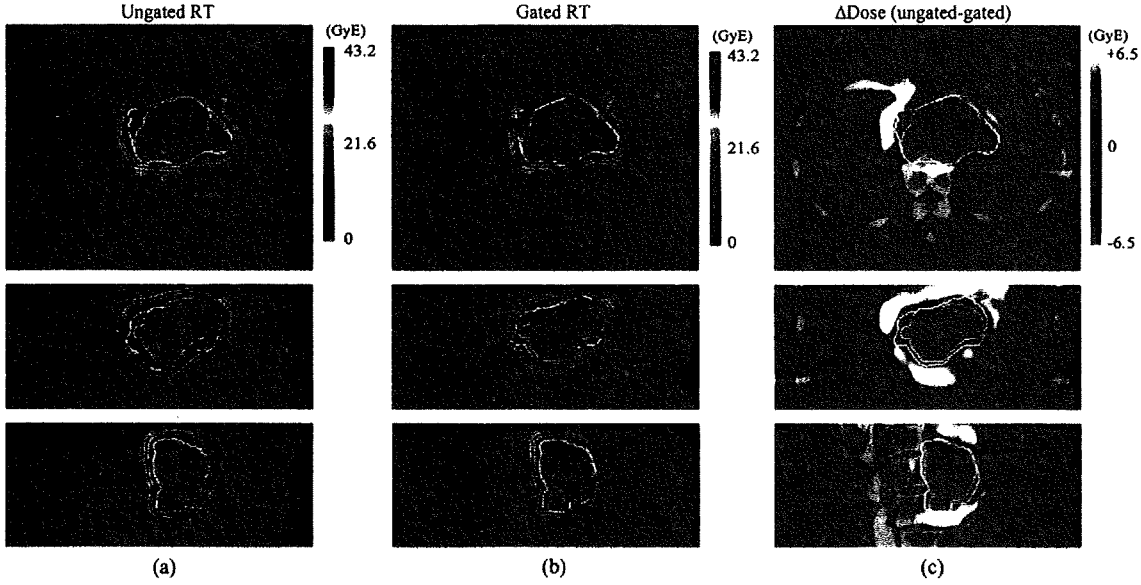

Fig. 4. Accumulated carbon ion beam dose distribution for (a) ungated treatment, (b) gated treatment, and (c) accumulated dose distribution differences (ungated minus gated) (Patient 1). Axial (upper row), coronal (middle row), and sagittal (lower row) sections. White areas, yellow areas, and dark green lines show the planning target volume (PTV), clinical target volume (CTV), and gross tumor volume (GTV) contours, respectively. Red, green, pink, light blue, and blue lines show 95%, 80%, 70%, 50%, and 30% of total doses, respectively.

respectively. The DVH curves for the duodenum at the middle dose were decreased from peak inhalation to peak exhalation. The 4D-DVH for the ungated and gated treatments in this patient were also closely similar (Fig. 7c).

Accumulated dose assessments for the ungated and gated treatments are summarized in Table 2. For both strategies, D95 values for the GTV and CTV were over 95% and delivered sufficient treatment beam. Maximum doses to the duodenum and pancreas averaged over all patients were 43.1/43.1GyE (ungated/gated) and 43.2/43.2GyE (ungated/gated), respectively, whereas V15 values for the kidney (right side/left side) averaged in all patients were 1.0%/10.9% and 0.8%/9.9%, respectively. The reason for the higher V15 values for the left than right kidney is that Patient 2 was irradiated from three beam directions, which did not include the right side.

Doses to other OARs were smaller in the gated than the ungated treatment, although the differences were small.

DISCUSSION

We compared respiratory-ungated and respiratory-gated strategies in pancreatic carbon ion beam treatment, which included intrafractional respiratory motion. Because rapid rotation CBCT improves 4DCT image quality over conventional multislice CT (MSCT), assessment was done on a quantitative basis. Results showed that because the compensating bolus was designed to cover the PTV, both treatment strategies delivered sufficient dose to the CTV and GTV. Gated treatment minimized excessive dosing to normal tissues over ungated treatment, although the differences were small.

Although the GTV and CTV moved up and down as a function of respiratory phase (Figs. 3 and 6), CTV movement in the posterior aspect was fixed, owing to the presence of the spine. Further, whereas the shape of the compensating bolus differed between the ungated and gated strategies, beam fields from the anterior direction were closely similar. As seen in Fig. 4c, accumulated dose distribution differences at the posterior side of the CTV were smaller than those at the anterior and inferior sides.

4DCT Imaging

Because of limitations in CT scan coverage in a single rotation, most 4DCTcquisition using conventional MSCT repeats a cine scan at each table position to acquire one respiratory cycle. Because respiratory amplitude is not always consistent across respiratory cycles, however, amplitude-based re-sorting is difficult. To account for this, re-sorting in 4DCT using conventional MSCT is done by subdividing one respiratory cycle into equal time intervals (phase-based sorting). In gated treatment, the treatment beam is usually irradiated based on the respiratory amplitude using the respiratory signal acquired from an external respiratory sensing system (*e.g.*, position-sensitive detector and revolutions per minute system) (27, 36). However, because the rapidly rotating CBCT used here scans approximately 12 cm in a single rotation and provides volumetric CT data with a coherent absolute time in all slices, re-sorting CT images at each slice position as a function of respiratory phase was not necessary. To approximate actual treatment conditions, we therefore subdivided a single respiratory cycle into 10 phases on the basis of respiratory amplitude.

The 4DCT obtained by the fast rotating CBCT provides more accurate geometric information than that by the conventional MSCT. However, because the duration of 4DCT imaging with the fast rotating CBCT is approximately 5 sec (~one respiratory cycle), these 4DCT images do not provide

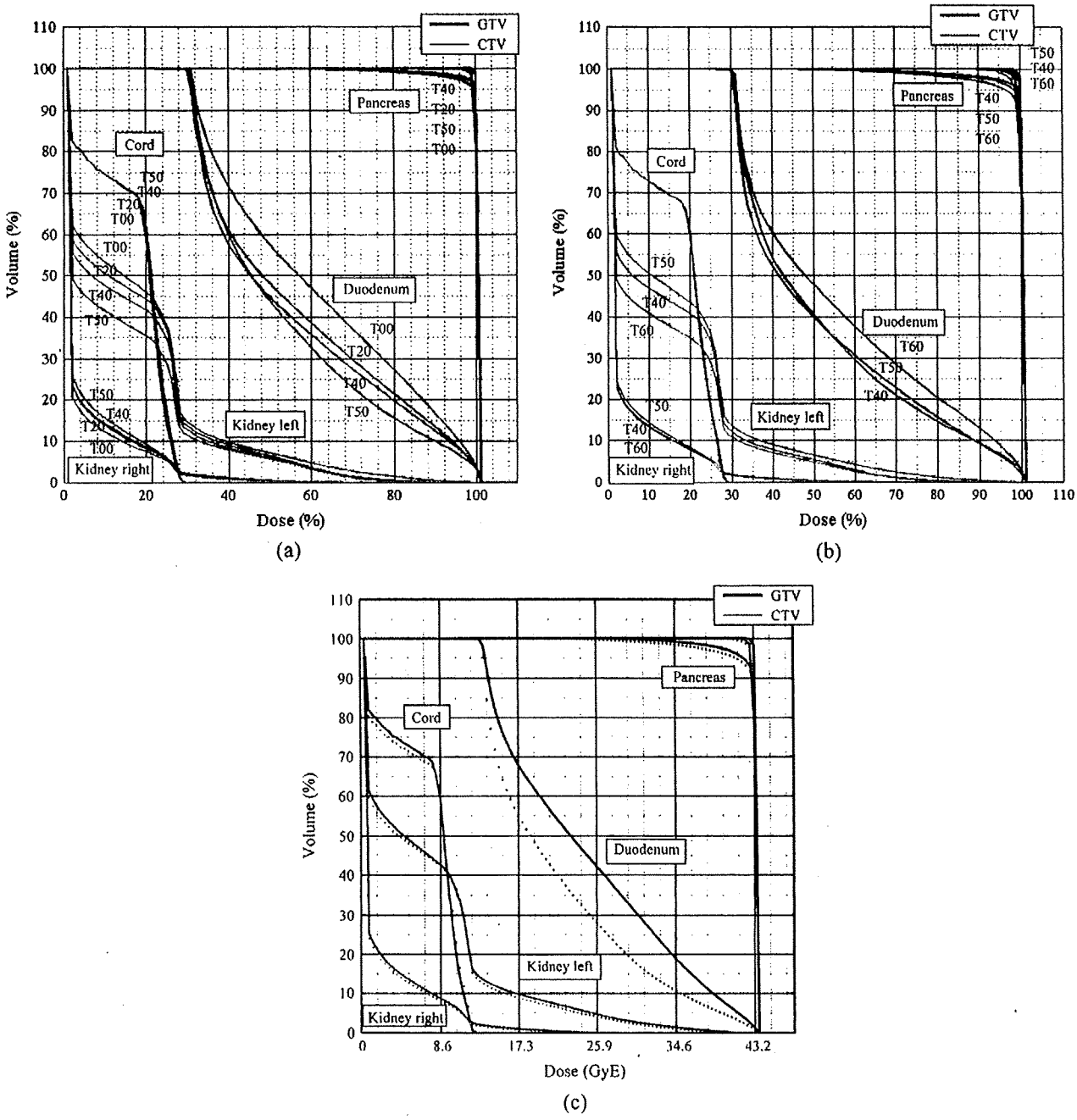

Fig. 5. Dose–volume histograms (DVHs) for (a) ungated and (b) gated treatments as a function of respiratory phase for Patient 1 (c) Four-dimensional DVH for ungated (solid line) and gated (dotted line) treatments. GTV = gross tumor volume; CTV = clinical target volume.

averaged patient breathing motion. By contrast, the duration of 4DCT imaging with the conventional MSCT is from tens of seconds to a few minutes, which is similar to the duration of treatment beam delivery, and therefore often provides an averaged picture of patient breathing motion. When MSCT with many slice detectors (64-slice CT) is used, however, the duration of 4DCT acquisition is shorter than that of treatment. Moreover, these 4DCT images may have decreased geometric accuracy because of the 4DCT artifacts. It is questionable whether 4DCT images obtained using a single conventional MSCT provide an accurate picture of a patient's averaged breathing motion. One possible solution to this problem is the acquisition of multiple 4DCT images over a few minutes.

Compensating bolus design

With regard to the bolus design algorithm, this was designed to provide stoppage of the charged particle beam at the distal edge of the CTV at each respiratory phase by accounting for intrafractional respiratory motion, on the basis that 4DCT images are subdivided on a respiratory phase basis

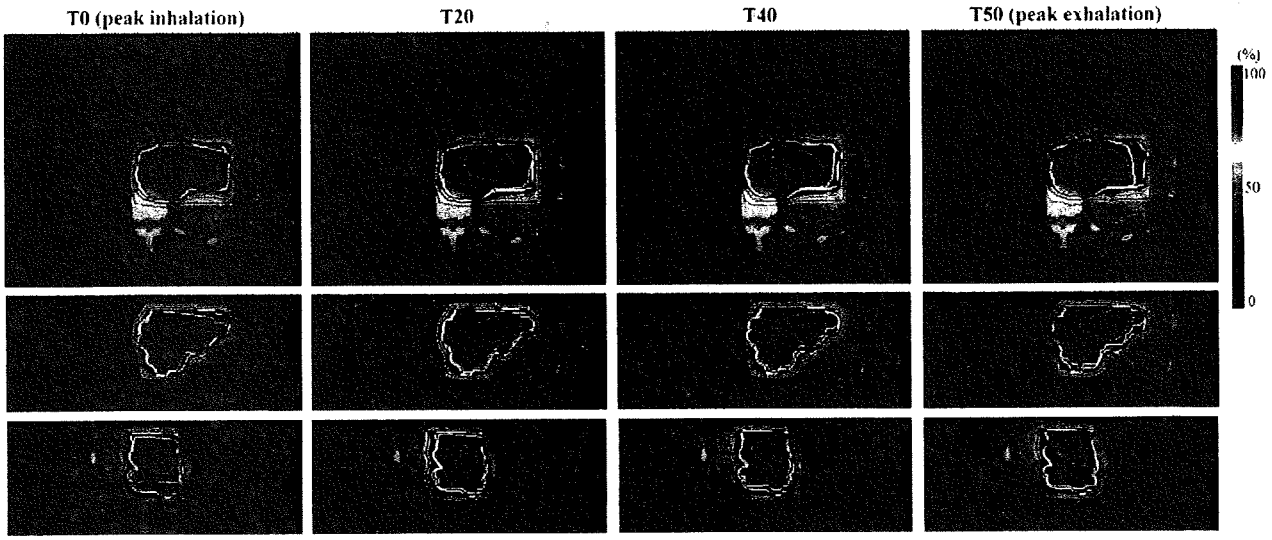

Fig. 6. Carbon ion beam dose distribution for ungated treatment (Patient 2). Axial (upper row), coronal (middle row), and sagittal (lower row) sections. White areas, yellow areas, and dark green lines show the planning target volume (PTV), clinical target volume (CTV), and gross tumor volume (GTV) contours, respectively. Red, green, pink, light blue, and blue lines show 95%, 80%, 70%, 50%, and 30% of total doses, respectively.

(periodic motion). The prescribed dose can therefore be delivered to the target at all respiratory phases without underdosing. A small overdose to the tissues may occur when the motion of a solid tumor or tissue leads it to be replaced by lower-density gas bowel during respiration. The present bolus was not optimized to account for involuntary gas bubble movement, however, which may in turn have degraded dose conformation to the target and increased dosing to the normal tissues. Because this study used a single 4DCT, we were unable to clarify whether these dose variations exerted any effect throughout a patient's treatment course.

Other bolus design approaches in proton beam treatment have been reported (21, 23). Kang *et al.* (23) applied an extended smearing grid size to time-averaged 4DCT data corresponding to intrafractional respiratory motion, whereas Engelsman *et al.* (21) used three 4DCT datasets. Our bolus design method differs from that of Kang *et al.* but is similar to that of Engelsman *et al.* Comparison of bolus design algorithms is beyond the scope of this study, which was rather aimed at comparing respiratory-ungated and respiratory-gated treatments in pancreatic cancer.

Dose assessment

In this study, we evaluated carbon ion beam dose distribution at respective phases and accumulated dose distribution by registering dose distributions at respective phases to peak exhalation using a deformable registration technique.

Statistical evaluation of dose assessment at each respiratory phase was useful in understanding dose variation due to intrafractional respiratory motion (Figs. 3, 5a and b, and 7a and b). As described above, however, because the 4DCT images were subdivided into 10 datasets by the amplitude-based re-sorting method, the absolute doses at each respiratory phase differed. Summarizing the statistical results of dose assessment at each respiratory phase for all patients is difficult. In clinical situations, moreover, the significant time requirements of dose assessment (*e.g.*, DVH) at each respiratory phase and the possibility of error makes accumulated dose assessment more practical. Although this situation is similar to that of current three-dimensional treatment planning, in which dose assessment at each beam field is useful in checking overdosage to normal tissues or underdosage to the target, most oncologists and physicists use the results of dose assessment for all beam fields combined in final decision making.

Several studies have shown that although respiratory pattern is periodic, it varies with each cycle: *e.g.*, position (amplitude) and cycle (37, 38). Here, however, we did not consider this variation in the accumulated dose calculation. Gating notwithstanding, respiratory positional variation (phase shift/drift) (38–42) may cause a decrease in the accumulated dose owing to movement of the target outside the beam field at a certain respiratory phase. This effect may have been enhanced in the present study because data for accumulated dose in gated treatment were averaged using three datasets (T40, T50, and T60) vs. 10 datasets (T0–T90) for ungated treatment. Even though respiratory pattern variation caused a decrease in dose delivery at a certain phase, the resulting decrease in accumulated dose may have been lower in the ungated than the gated treatment as a result of averaging of the accumulated dose in the region.

Given that our results for ungated and gated pancreatic treatment were closely similar with regard to tolerance doses to normal tissues, and that doses were less than the tolerance dose in both ungated and gated treatments, and taking into account the above problem, we suggest that ungated pancreatic treatment may deliver sufficient accumulated dose through

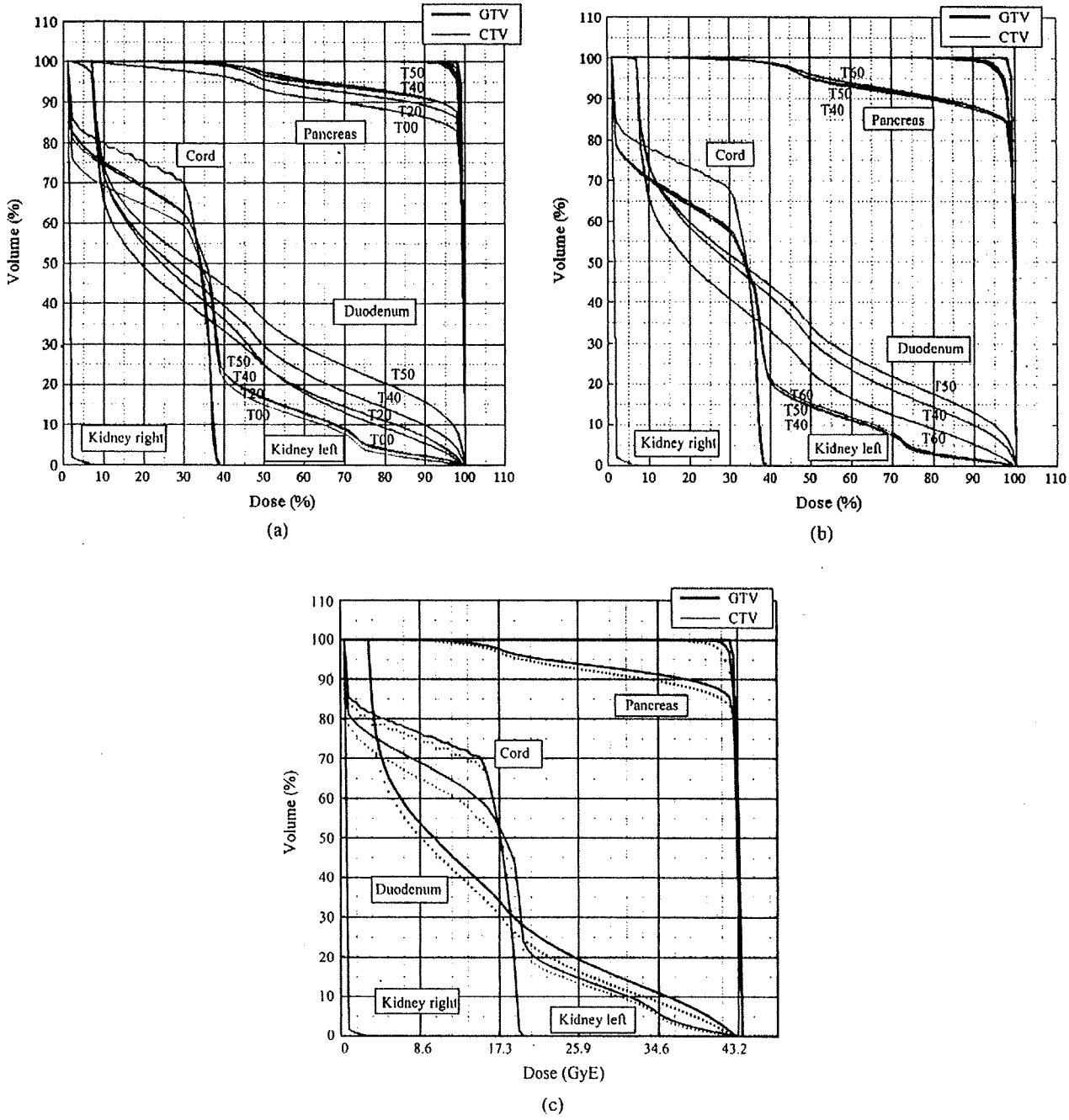

Fig. 7. Dose–volume histograms (DVHs) for (a) ungated and (b) gated treatments as a function of respiratory phase for Patient 2 (c) Four-dimensional DVH for ungated (solid line) and gated (dotted line) treatments. GTV = gross tumor volume; CTV = clinical target volume.

the treatment course with minimal dose variation due to respiratory pattern variation, and in this regard is therefore preferable to gated treatment. The use of ungated treatment may shorten total treatment duty time by a factor of three compared with gated treatment.

In this study we did not consider patient condition, particularly with regard to the possibility that chemotherapy might have increased excessive dosing to gastrointestinal organs in ungated treatment. Any application of our results to clinical use should therefore be undertaken only after discussion with oncologists, particularly with regard to radiotherapy combined with chemotherapy.

CONCLUSION

The present study was conducted to compare respiratory-gated and respiratory-ungated treatment in patients with pancreatic cancer using a scattered carbon ion beam. Although gating minimized excessive dosing to normal tissues, the difference between the strategies was small.

Table 2. Accumulated dose assessment for ungated and gated treatments

Pt. no.	Strategy	GTV D95(%)	CTV D95(%)	Cord Dmax (GyE)	Kidney-Right			Kidney-Left			Duodenum			Pancreas		
					Dmax(GyE)	v30(%)	v15(%)	Dmax(GyE)	v30(%)	v15(%)	Dmax(GyE)	v40(%)	v20(%)	Dmax(GyE)	v40(%)	v20(%)
1	Upgate	98.0	97.2	11.7	27.2	1.4	1.4	42.3	2.8	11.4	43.2	7.0	59.2	43.2	97.2	100.0
	Gate	98.0	97.1	11.7	25.9	0.0	1.2	42.3	2.3	10.5	43.2	4.4	45.5	43.2	96.0	100.0
2	Upgate	97.0	96.2	19.0	2.2	0.0	0.0	42.7	11.3	59.6	42.7	4.7	28.0	43.2	88.5	96.0
	Gate	97.0	94.9	19.0	2.6	0.0	0.0	42.7	10.3	54.6	42.7	3.3	24.5	43.2	86.5	95.1
3	Upgate	97.1	95.4	12.1	31.1	0.8	0.8	26.3	0.0	1.3	43.2	3.4	23.6	43.2	69.2	86.8
	Gate	97.0	94.6	12.1	29.4	0.0	0.7	25.9	0.0	1.0	43.2	3.2	21.6	43.2	68.3	86.6
4	Upgate	97.1	97.0	12.1	22.0	0.0	0.0	30.2	0.0	0.8	43.2	6.3	36.4	43.2	77.4	89.1
	Gate	97.2	95.6	12.1	12.5	0.0	0.0	26.3	0.0	0.2	43.2	3.4	30.5	43.2	68.6	82.3
5	Upgate	98.1	96.9	13.0	25.9	2.2	2.2	27.2	0.0	1.6	43.2	4.5	28.0	43.2	79.9	87.9
	Gate	98.0	96.0	13.4	25.5	0.0	2.0	27.6	0.0	1.4	43.2	3.2	22.9	43.2	78.6	87.3
6	Upgate	98.1	97.1	11.2	25.9	2.0	2.0	35.4	0.1	1.9	43.2	13.0	45.6	43.2	69.1	81.5
	Gate	98.0	96.5	11.2	24.6	0.0	1.8	31.5	0.0	1.5	43.2	10.0	41.6	43.2	66.0	79.1
7	Upgate	97.2	96.2	11.7	26.4	0.8	0.8	20.7	0.0	0.1	43.2	11.3	43.7	43.2	73.0	95.1
	Gate	97.5	93.3	11.7	23.3	0.0	0.2	21.1	0.0	0.1	43.2	10.5	33.6	43.2	75.1	93.1
Average	Upgate	97.5	96.6	13.0	23.0	1.0	1.0	32.1	2.0	10.9	43.1	7.2	37.8	43.2	79.2	90.9
	Gate	97.5	95.4	13.0	20.6	0.0	0.8	31.1	1.8	9.9	43.1	5.4	31.5	43.2	77.0	89.0

Abbreviations: Pt. no. = patient number; GTV = gross tumor volume; CTV = clinical target volume.

Respiratory gating may therefore not always be necessary in pancreatic treatment as long as dose distribution is assessed. Allowing for our limited number of patients, our quantitative results may help improve treatment accuracy in charged particle pancreatic therapy in clinical treatment. We intend to extend this study of 4D carbon ion beam treatment in the pancreatic region to other abdominal regions (*e.g.*, liver, kidney, prostate).

REFERENCES

1. Mori S, Chen GT, Endo M. Effects of intrafractional motion on water equivalent pathlength in respiratory-gated heavy charged particle beam radiotherapy. *Int J Radiat Oncol Biol Phys* 2007; 69:308–317.
2. Mori S, Wolfgang J, Lu HM, *et al.* Quantitative assessment of range fluctuations in charged particle lung irradiation. *Int J Radiat Oncol Biol Phys* 2008;70:253–261.
3. Lattanzi J, McNeeley S, Pinover W, *et al.* A comparison of daily CT localization to a daily ultrasound-based system in prostate cancer. *Int J Radiat Oncol Biol Phys* 1999;43: 719–725.
4. Hong L, Goitein M, Bucciolini M, *et al.* A pencil beam algorithm for proton dose calculations. *Phys Med Biol* 1996;41: 1305–1330.
5. Seiler PG, Blattmann H, Kirsch S, *et al.* A novel tracking technique for the continuous precise measurement of tumour positions in conformal radiotherapy. *Phys Med Biol* 2000;45: N103–N110.
6. Roach M 3rd, Faillace-Akazawa P, Malfatti C, *et al.* Prostate volumes defined by magnetic resonance imaging and computerized tomographic scans for three-dimensional conformal radiotherapy. *Int J Radiat Oncol Biol Phys* 1996;35: 1011–1018.
7. Britton KR, Starkschall G, Tucker SL, *et al.* Assessment of gross tumor volume regression and motion changes during radiotherapy for non-small-cell lung cancer as measured by four-dimensional computed tomography. *Int J Radiat Oncol Biol Phys* 2007;68:1036–1046.
8. Seppenwoolde Y, Shirato H, Kitamura K, *et al.* Precise and real-time measurement of 3D tumor motion in lung due to breathing and heartbeat, measured during radiotherapy. *Int J Radiat Oncol Biol Phys* 2002;53:822–834.
9. Chen QS, Weinhous MS, Deibel FC, *et al.* Fluoroscopic study of tumor motion due to breathing: facilitating precise radiation therapy for lung cancer patients. *Med Phys* 2001;28: 1850–1856.
10. Bert C, Saito N, Schmidt A, *et al.* Target motion tracking with a scanned particle beam. *Med Phys* 2007;34:4768–4771.
11. Keall PJ, Cattell H, Pokhrel D, *et al.* Geometric accuracy of a real-time target tracking system with dynamic multileaf collimator tracking system. *Int J Radiat Oncol Biol Phys* 2006;65: 1579–1584.
12. Keall PJ, Kini VR, Vedam SS, *et al.* Motion adaptive x-ray therapy: A feasibility study. *Phys Med Biol* 2001;46:1–10.
13. Lu W. Real-time motion-adaptive delivery (MAD) using binary MLC: I. Static beam (topotherapy) delivery. *Phys Med Biol* 2008;53:6491–6511.
14. McMahon R, Berbeco R, Nishioka S, *et al.* A real-time dynamic-MLC control algorithm for delivering IMRT to targets undergoing 2D rigid motion in the beam's eye view. *Med Phys* 2008;35:3875–3888.
15. Papiez L, Rangaraj D. DMLC leaf-pair optimal control for mobile, deforming target. *Med Phys* 2005;32:275–285.
16. Tacke M, Nill S, Oelfke U. Real-time tracking of tumor motions and deformations along the leaf travel direction with the aid of

a synchronized dynamic MLC leaf sequencer. *Phys Med Biol* 2007;52:N505–N512.
17. Sontag M. Respiratory gated radiotherapy. *Med Phys* 1999;26: 1112–1113.
18. Minohara S, Kanai T, Endo M, *et al.* Respiratory gated irradiation system for heavy-ion radiotherapy. *Int J Radiat Oncol Biol Phys* 2000;47:1097–1103.
19. Ohara K, Okumura T, Akisada M, *et al.* Irradiation synchronized with respiration gate. *Int J Radiat Oncol Biol Phys* 1989;17:853–857.
20. Mori S, Sharp GC, Kumagai M, *et al.* Four-dimensional heavy charged particle beam radiotherapy in pancreatic cancer. *Int J Radiat Oncol Biol Phys* 2008;72:S541.
21. Engelsman M, Rietzel E, Kooy HM. Four-dimensional proton treatment planning for lung tumors. *Int J Radiat Oncol Biol Phys* 2006;64:1589–1595.
22. Rietzel E, Liu AK, Doppke KP, *et al.* Design of 4D treatment planning target volumes. *Int J Radiat Oncol Biol Phys* 2006; 66:287–295.
23. Kang Y, Zhang X, Chang JY, *et al.* 4D Proton treatment planning strategy for mobile lung tumors. *Int J Radiat Oncol Biol Phys* 2007;67:906–914.
24. Zhao L, Sandison GA, Farr JB, *et al.* Dosimetric impact of intrafraction motion for compensator-based proton therapy of lung cancer. *Phys Med Biol* 2008;53:3343–3364.
25. Bert C, Rietzel E. 4D treatment planning for scanned ion beams. *Radiat Oncol* 2007;2:24.
26. Chen GT, Kung JH, Rietzel E. Four-dimensional imaging and treatment planning of moving targets. *Front Radiat Ther Oncol* 2007;40:59–71.
27. Keall PJ, Kini VR, Vedam SS, *et al.* Potential radiotherapy improvements with respiratory gating. *Australas Phys Eng Sci Med* 2002;25:1–6.
28. Endo M, Mori S, Kandatsu S, *et al.* Development of real 4D CT with real-time reconstruction and display. *IEEE NSS/MIC Conf Record* 2006;M11–M252.
29. Mori S, Endo M, Tsunoo T, *et al.* Physical performance evaluation of a 256-slice CT-scanner for four-dimensional imaging. *Med Phys* 2004;31:1348–1356.
30. Olsen JR, Lu W, Hubenschmidt JP, *et al.* Effect of novel amplitude/phase binning algorithm on commercial four-dimensional computed tomography quality. *Int J Radiat Oncol Biol Phys* 2008;70:243–252.
31. Wink N, Panknin C, Solberg TD. Phase versus amplitude sorting of 4D-CT data. *J Appl Clin Med Phys* 2006;7:77–85.
32. Sharp GC, Kandasamy N, Singh H, *et al.* GPU-based streaming architectures for fast cone-beam CT image reconstruction and demons deformable registration. *Phys Med Biol* 2007;52: 5771–5783.
33. International Electrotechnical Commission, Radiotherapy equipment: Cordinates, movements and scales. *Pub IEC* 2002;61217.
34. Kanai T, Endo M, Minohara S, *et al.* Biophysical characteristics of HIMAC clinical irradiation system for heavy-ion radiation therapy. *Int J Radiat Oncol Biol Phys* 1999;44:201–210.
35. Petti PL. Differential-pencil-beam dose calculations for charged particles. *Med Phys* 1992;19:137–149.
36. Ford EC, Mageras GS, Yorke E, *et al.* Evaluation of respiratory movement during gated radiotherapy using film and electronic portal imaging. *Int J Radiat Oncol Biol Phys* 2002;52:522–531.
37. Lujan AE, Balter JM, Ten Haken RK. A method for incorporating organ motion due to breathing into 3D dose calculations in the liver: Sensitivity to variations in motion. *Med Phys* 2003;30: 2643–2649.
38. Korreman SS, Juhler-Nottrup T, Boyer AL. Respiratory gated beam delivery cannot facilitate margin reduction, unless combined with respiratory correlated image guidance. *Radiother Oncol* 2008;86:61–68.
39. Russell KR, Isacsson U, Saxner M, *et al.* Implementation of pencil kernel and depth penetration algorithms for treatment planning of proton beams. *Phys Med Biol* 2000;45:9–27.
40. Koch N, Liu HH, Starkschall G, *et al.* Evaluation of internal lung motion for respiratory-gated radiotherapy using MRI: Part I: Correlating internal lung motion with skin fiducial motion. *Int J Radiat Oncol Biol Phys* 2004;60:1459–1472.
41. Hoisak JD, Sixel KE, Tirona R, *et al.* Correlation of lung tumor motion with external surrogate indicators of respiration. *Int J Radiat Oncol Biol Phys* 2004;60:1298–1306.
42. Liu HH, Koch N, Starkschall G, *et al.* Evaluation of internal lung motion for respiratory-gated radiotherapy using MRI: Part II. Margin reduction of internal target volume. *Int J Radiat Oncol Biol Phys* 2004;60:1473–1483.

Radiotherapy and Oncology xxx (2009) xxx–xxx

Contents lists available at ScienceDirect

Radiotherapy and Oncology

journal homepage: www.thegreenjournal.com

Original article

Dose–volume histogram and dose–surface histogram analysis for skin reactions to carbon ion radiotherapy for bone and soft tissue sarcoma

Takeshi Yanagi *, Tadashi Kamada, Hiroshi Tsuji, Reiko Imai, Itsuko Serizawa, Hirohiko Tsujii

Research Center Hospital for Charged Particle Therapy, National Institute of Radiological Sciences, Chiba, Japan

ARTICLE INFO

Article history:
Received 17 March 2009
Received in revised form 24 August 2009
Accepted 27 August 2009
Available online xxxx

Keywords:
Dose–volume histogram
Dose–surface histogram
Carbon ion radiotherapy
Bone and soft tissue sarcoma
Skin reaction
Skin ulcer

ABSTRACT

Background and purpose: To evaluate the usefulness of the dose–volume histogram (DVH) and dose–surface histogram (DSH) as clinically relevant and available parameters that helped to identify bone and soft tissue sarcoma patients at risk of developing late skin reactions, including ulceration, when treated with carbon ion radiotherapy.

Materials and methods: Thirty-five patients with bone and soft tissue sarcoma treated with carbon ion beams were studied. The clinical skin reactions were evaluated. Some pretreatment variables were compared with the grade of late skin reactions.

Results: Average DVH and DSH were established in accordance with the grading of the skin reactions. Prescribed dose, the difference in depths between the skin surface and the proximal extent of the tumor, and some DVH/DSH parameters were correlated with late skin reaction (≧grade 3) according to univariate analysis. Furthermore, the area irradiated with over 60 GyE (S_{60} > 20 cm^2) on DSH was the most important factor by multivariate analysis.

Conclusions: The area irradiated with over 60 GyE (S_{60} > 20 cm^2) on DSH was found to be a parameter for use as a predictor of late skin reactions.

 Radiotherapy and Oncology xxx (2009) xxx–xxx

In 1994, clinical research trials using carbon ion beams were initiated at the National Institute of Radiological Sciences (NIRS) in Chiba, Japan [1–3]. As of February 2008, a total of 3819 patients (4053 lesions) have been treated by this modality. Some of these patients, especially those with bone and soft tissue sarcoma, had tumors located near the skin and developed severe skin reactions after treatment [3]. Among them, some progressed to grade 4 late skin reactions identified as ulcers. To allow the prediction of such skin reactions, it is useful to search for factors that are related to the skin reactions. Thus, in this study, certain factors of patients with bone and soft tissue sarcoma were assessed in terms of correlation with late skin reactions associated with the clinical use of carbon ion radiotherapy.

Materials and methods

Protocol study

From June 1996 to December 1999, 64 lesions in 57 patients (37 men and 20 women) with unresectable bone and soft tissue sarcoma were treated with carbon ion beams according to our dose escalation protocol. The patient eligibility of this protocol was described previously [3]. Briefly, they had histologically confirmed bone and soft tissue sarcomas judged unresectable by the referring surgeon. The tumor had to be grossly measurable, but its size was not allowed to exceed 15 cm. For dose escalation, at least 3 patients each were treated at the same dose level, and then, after careful observation, a 10% total-dose escalation was conducted. All patients signed informed consent forms approved by the local institutional review board.

Patient selection criteria

For the sake of accuracy and simplicity of evaluation, the following patients were excluded from the analysis: (1) those with tumor invasion into the skin, which might complicate the direct radiation effect on the skin; (2) those who died within six months (in the case of acute skin evaluation) or within 1.5 years (in the case of late skin evaluation) after treatment; (3) those treated in both supine and prone positions because they required recalculation of the total dose of both positions using a pseudo-target; and (4) those with tumors located in a limb, because skin reactions of limbs show different patterns from those of other sites, and should be dealt with separately. After these adjustments, 35 patients (35 lesions) were analyzed for acute skin reactions and 27 of these patients (27 lesions) were also analyzed for late skin reactions.

* Corresponding author. Address: Research Center Hospital for Charged Particle Therapy, National Institute of Radiological Sciences, Anagawa 4-9-1, Inage Ward, Chiba City, Chiba Prefecture 263-8555, Japan.
E-mail address: tyana@med.nagoya-cu.ac.jp (T. Yanagi).

0167-8140/$ - see front matter © 2009 Elsevier Ireland Ltd. All rights reserved.
doi:10.1016/j.radonc.2009.08.041

Please cite this article in press as: Yanagi T et al. Dose–volume histogram and dose–surface histogram analysis for skin reactions to carbon ion radiotherapy for bone and soft tissue sarcoma. Radiother Oncol (2009), doi:10.1016/j.radonc.2009.08.041

Carbon ion radiotherapy

Carbon ion beams were generated by HIMAC (Heavy Ion Medical Accelerator in Chiba), the world's first heavy ion accelerator complex dedicated to medical use in a hospital environment [1]. The energy levels of the generated beams were 290 MeV, 350 MeV, and 400 MeV. For the treatment, the patients were positioned in customized cradles (Moldcare; Alcare, Tokyo, Japan) and were immobilized with a low-temperature thermoplastic retaining device. A set of 5-mm-thick slice CT images was taken for treatment planning with the patients retained in the immobilization device. Three-dimensional treatment planning was performed using HIPLAN software (by NIRS) [4].

In accordance with the ICRU Report [5], the visible lesion on the CT image was defined as the gross tumor volume (GTV). The clinical target volume (CTV) included the GTV and the estimated subclinical local involvement. An internal margin was added to the CTV to allow for tumor movement and tumor growth. The planning target volume (PTV) consisted of the CTV, the internal margin, and a set-up margin corresponding to the sum of the error lengths at positioning (about half the length of the CT slice thickness in our system) including the dose calculation error associated with the change from the CT value to the beam range (about 3% at our system). As a result, a margin of about 5 mm was usually added to the CTV to create the PTV. The PTV was covered by at least 90% of the administered dose.

Dose was expressed in Gray equivalent (GyE), which was calculated by multiplying the physical dose with the Relative Biological Effectiveness (RBE). The RBE was estimated to be 3.0 at the distal part of the spread-out Bragg peak (SOBP) based upon radiobiological studies. The details of the RBE value used at NIRS were discussed by Kanai et al. [6].

Skin evaluation

Four radiation oncologists score-rated all the skin reactions of each patient in the maximum phase by checking the photo-slides captured during the follow-up durations, using the RTOG Scoring System for assessing acute reactions and the Late Radiation Morbidity Scoring Scheme of RTOG/EORTC for evaluating the late skin reactions [7].

Dose-volume histogram (DVH) and dose-surface histogram (DSH)

DVH was calculated for the region of interest (ROI). ROI was defined as all the organs inside the body covered by the skin at the irradiated area. DSH was calculated by the following procedure. First, the skin contours were carefully outlined with a thickness of one pixel for each CT slice. Then, the contours of the skin surface on each CT slice were divided into small (5 mm) compartments, and multiplied by the thickness of the CT slice (5 mm). In this manner, a number of 25-mm^2 square-shaped compartments with one-pixel-sized-thickness volume were made. The next step was to calculate the radiation dose delivered to each of these compartments. The equal-dose compartments were then summated to determine the cumulative area irradiated with each discrete dose level so as to obtain the cumulative DSH. The calculation of DVH and DSH was performed using HIPLAN software [4].

Evaluation of pretreatment variables

Some of the pretreatment variables thought to be relevant to late skin reactions were assessed using Fisher's exact test in univariate analysis. The variables contained sex, patient age, primary tumor site, difference in depths between the skin surface and the proximal extent of the tumor, planning target volume, prescribed dose, neoadjuvant chemotherapy, and adjuvant chemotherapy. Furthermore, some factors with significance in univariate analysis and the representative values derived from DVH/DSH parameters were applied to multivariate analysis using Cox's proportional hazard model.

Results

Patient and tumor characteristics

All 35 patients with acute skin reactions and 27 patients with late skin reactions were analyzed. The number of lesions and patients was the same. Table 1 shows the patients' and tumor characteristics. The numbers of patients at each total-dose level were 3 (52.8 GyE), 6 (57.6 GyE), 6 (64 GyE), 5 (70.4 GyE), and 15 (73.6 GyE) for acute skin reactions, and 3 (52.8 GyE), 3 (57.6 GyE), 5 (64 GyE), 4 (70.4 GyE), and 12 (73.6 GyE) for late skin reactions. All the patients were treated in fixed 16 fractions. In the patients analyzed for late skin reactions, more than one-third of the tumors were located in the sacral region.

Follow-up and skin reactions

After the treatment, the patients were examined on a regular basis throughout the follow-up period. Maximum follow-up time in these patients ranged from 29.5 to 71.7 months (median 44.7 months).

Table 1
Patients' and tumor characteristics.

	Acute evaluation	Late evaluation
Numbers	35	27
Age/median (years)	15–85/47	15–85/51
Gender		
Male	22 (62.9%)	18 (66.7%)
Female	13 (37.1%)	9 (33.3%)
Tumor site		
Sacrum	11 (31.4%)	10 (37.0%)
Spine	10 (28.6%)	8 (29.6%)
Iliac bone	6 (17.1%)	3 (11.1%)
Pubic bone	4 (11.4%)	3 (11.1%)
Others	4 (11.4%)	4 (11.1%)
Target volume/median (ml)	49–1829/714	49–1665/701
Target dose		
52.8 GyE	3 (8.6%)	3 (11.1%)
57.6 GyE	6 (17.1%)	3 (11.1%)
64.0 GyE	6 (17.1%)	5 (18.5%)
70.4 GyE	5 (14.3%)	4 (14.8%)
73.6 GyE	15 (42.9%)	12 (44.4%)
Histologic diagnosis		
Bone		
Osteosarcoma	9 (25.7%)	8 (30.0%)
Chordoma	9 (25.7%)	9 (33.3%)
Chondrosarcoma	3 (18.6%)	2 (7.4%)
Others	3 (18.6%)	0 (0%)
Soft tissue		
MPNST[a]	4 (11.4%)	2 (7.4%)
MFH[b]	1 (2.9%)	0 (0%)
Liposarcoma	1 (2.9%)	1 (3.7%)
Others	5 (14.3%)	5 (18.5%)
Chemotherapy		
Neoadjuvant (+)	19 (54.3%)	14 (51.9%)
Neoadjuvant (−)	16 (45.7%)	13 (48.1%)
Adjuvant (+)	8 (22.9%)	6 (22.2%)
Adjuvant (−)	27 (77.1%)	21 (77.8%)

[a] Malignant peripheral nerve sheath tumor.
[b] Malignant fibrous histocytoma.

The outcome of the skin reactions is presented in Tables 2 and 3. Four patients developed late grade 4 skin reactions (ulceration). Patients who developed grade 3 or 4 late skin reactions had been prescribed with 70.4 GyE or more to the PTV. Three out of 4 patients who indicated grade 4 late skin reactions had the tumor located in the sacrum. The site of the skin reactions of these patients was at the gluteal fold.

The time of onset of late grade 3 varied from 6 months to 29 months, and that of late grade 4 varied from 8 months to 21 months after the initiation of the irradiation. The patients developing ulceration corresponding to a late grade 4 skin reaction needed surgery for recovery.

Dose–volume histogram and dose–surface histogram

In the dose–volume histograms and dose–surface histograms, the patients who received relatively high doses to their volumes or areas developed grade 3 or 4 reactions. DSH for all the patients graded by acute skin reaction is shown in Fig. 1. In order to understand their general trend, the average DVHs for some grade groups – grade 0 + 1, grade 2, grade 3, and grade 4 – for acute and late skin reactions are presented (figure for late skin reaction is shown in Fig. 2). There was a tendency for the curves to be separated from each other on the high dose side, which was above 56 GyE with regard to acute reactions (figure is not shown) and above 52 GyE with respect to late reactions. Concerning DSH, when we divided the patients into three groups, namely grade 0 + 1, grade 2, and grade 3 + 4, the average area for patients with acute and late grades 3 + 4 reactions was above the corresponding values for patients with grades 0 + 1 and/or grade 2 in almost all the graphs (figure for late reaction is shown in Fig. 3).

To find the representative parameters of the DVH values to use for the prediction of the late skin reaction, at first, the correlation between cumulative irradiated volume value sets at every dose in 2-GyE increments from 2 GyE to 74 GyE (V_2–V_{74}) of DVH and the grades of the late skin reactions (≧grade 3 vs. <grade 3) were evaluated by a nonparametric test, the Spearman's correlation test. The results showed that the values of V_{64} and V_{68} were correlated with the late skin reactions and became candidates for prognostic parameters. In the same manner, the values between S_{56} and S_{64} were derived from DSH as candidates. Then, we set the "cut-off volume" or "cut-off surface area" for each representative value at 100 ml or 10 cm^2 increments, which divided the lesions (patients) into two groups – above and below the cut-off levels. Then, the DVH or DSH parameters grouped by each cut-off level and late clinical reaction were evaluated. Finally, the $V_{64} > 100$ ml for DVH, and $S_{60} > 20$ cm^2 for DSH were selected as the candidates for predicting late skin reactions.

As for the consequential correlation between DVH/DSH and skin reaction achieved, the probability of grade 3 late skin reaction in patients with $V_{64} > 100$ ml and $V_{64} \leqslant 100$ ml was 60% and 8.3%, respectively, while that in patients with $S_{60} > 20$ cm^2 and $S_{60} \leqslant 20$ cm^2 was 100% and 22.7%, respectively.

Prognostic factors

On univariate analysis, the prescribed dose and the difference in depths between the skin surface and the proximal extent of the tumor were correlated with the development of late skin reactions (Table 4). On multivariate analysis among the difference in depths between the skin and the tumor, and the DVH/DSH parameters, the DSH parameter $S_{60} > 20$ cm^2 showed statistical significance ($p = 0.041$) (Table 5).

Correlation of acute skin and late skin reactions

In terms of the correlation between the grades of acute and late skin reactions, it was found that all lesions showed the same grade or a 1-grade difference between early and late reactions except for one lesion with a 2-grade difference (Fig. 4). Furthermore, among the four patients who developed late skin ulcerations, one patient failed to heal the acute moist desquamation and directly progressed into a late phase of the skin reaction.

Table 2
Outcome of skin reactions (1).

Dose (GyE)	Acute skin reaction						Late skin reaction					
	Grade of RTOG					Total	Grade of RTOG/EORTC					Total
	0	1	2	3	4		0	1	2	3	4	
52.8	0	2	1	0	0	3	0	2	1	0	0	3
57.6	0	2	4	0	0	6	0	3	0	0	0	3
64.0	1	4	1	0	0	6	1	3	1	0	0	5
70.4	0	1	2	2	0	5	0	1	0	2	1	4
73.6	0	2	7	5	1	15	0	3	2	4	3	12
Total	1	11	15	7	1	35	1	12	4	6	4	27

Table 3
Outcome of skin reactions (2).

Site	Acute skin reaction						Late skin reaction					
	Grade of RTOG					Total	Grade of RTOG/EORTC					Total
	0	1	2	3	4		0	1	2	3	4	
Sacrum	0	1	4	6	0	11	0	1	3	3	3	10
Spine	1	4	4	1	0	10	1	4	1	2	0	8
Iliac bone	0	1	4	0	1	6	0	1	0	1	1	3
Pubic bone	0	2	2	0	0	4	0	3	0	0	0	3
Others	0	3	1	0	0	4	0	3	0	0	0	3
Total	1	11	15	7	1	35	1	12	4	6	4	27

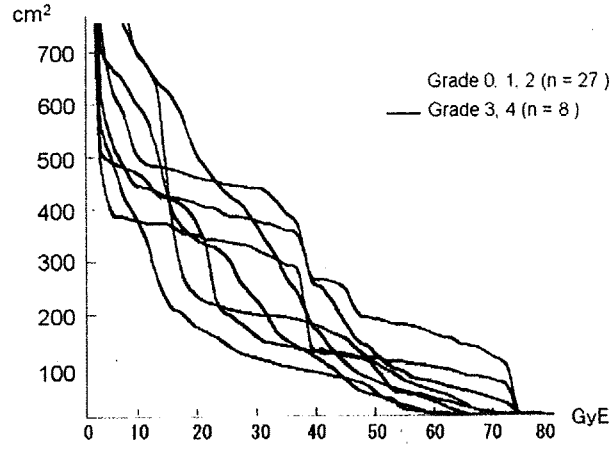

Fig. 1. DSH for all the patients grading by acute skin reaction (grade 0 + 1 + 2 vs. grade 3 + 4). In the dose-surface histograms, the patients who received relatively high doses to their surface area indicated grade 3 or 4 reactions.

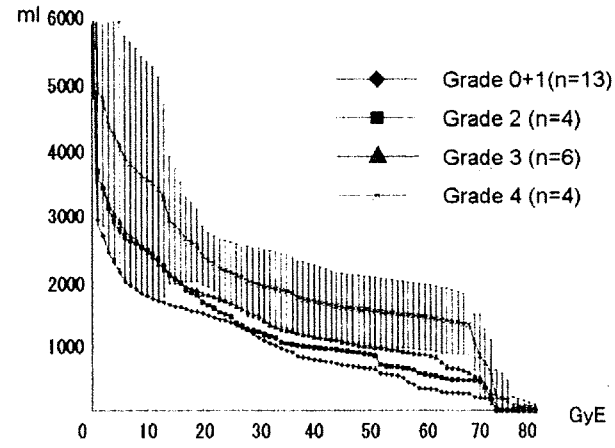

Fig. 2. Average DVH grading by late skin reactions (with the standard error bar of grade 4 reactions). There is a tendency for the curves to be separated from each other in the higher-dose part between 52 GyE and 74 GyE with respect to late reactions ($n = 27$).

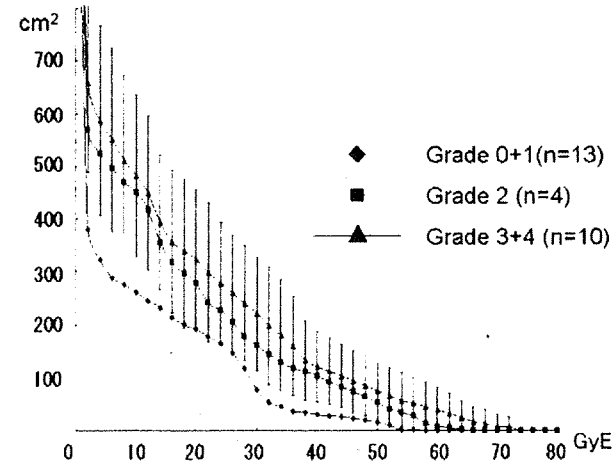

Fig. 3. Average DSH grading by late skin reactions (with the standard error bar of grade 3 + 4 reactions). The curves were also separated from each other throughout the whole dose part of the graph ($n = 27$).

Table 4
Univariate analysis (late reactions ⩾ grade 3).

		odds ratio (95% CI)
Sex	(M, F)	1.27 (0.23–6.82)
Age	(⩾55 year,<55 year)	2.4 (0.47–12.13)
Primary tumor site	(Sacrum, other)	4.87 (0.89–26.42)
Planning target volume	(⩾900 ml,<900 ml)	3.11 (0.52–18.38)
Prescribed dose	(⩾70.4 GyE,<70.4 GyE)*	–
Neoadjuvant chemotherapy	(+, −)	0.88 (0.18–4.24)
Adjuvant chemotherapy	(+, −)	5 (0.71–34.91)
Difference in depths[a]	(<2 cm,⩾2 cm)*	10.12 (1.04–98.49)

[a] Difference in depths between skin and tumor.
* p Value < 0.05.

Table 5
Multivariate analysis (late reactions ⩾ grade 3).

	p Value	Hazard ratio	CI (95%)
Difference in depth between skin and tumor	0.657	1.669	0.174–15.998
Dose-volume histogram (V_{64} > 100 ml)	0.189	4.743	0.466–48.284
Dose-surface histogram (S_{60} > 20 cm²)	0.041*	5.107	1.068–24.420

Cox hazard model.
* p Value < 0.05.

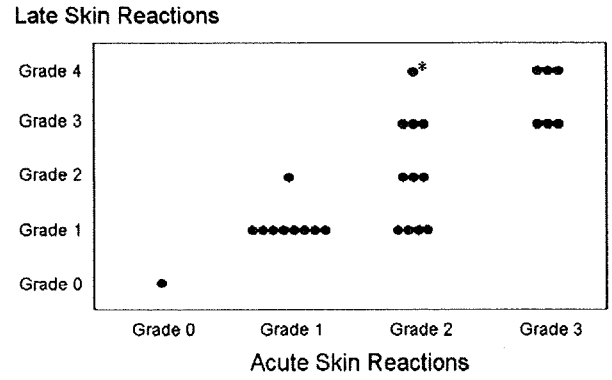

Fig. 4. Correlation between the grades of acute and late skin reactions. All patients showed the same grade or a 1-grade difference between early and late reactions except for one patient (*) with a 2-grade difference.

Discussion

In this study, acute and late skin reactions of the patients with bone and soft tissue sarcoma treated with carbon ion beams were evaluated, and a parameter for use as a predictor of late skin reactions was proposed.

In general, skin reactions to radiotherapy are divided into acute phase and late phase reactions. In acute radiation dermatitis the parenchyma of the skin, i.e., the epidermis, plays a leading role, and in the chronic phase it is the dermis and the subcutis that dominate the radiation injury to the skin. In terms of the degree of the normal tissue reaction, it is known that this is connected with the volume effect. Animal experiments have shown that the size of the irradiated field is associated with the intensity of the skin reactions [8]. Furthermore, the highly significant increase in incidence and severity was reported with increasing field size in the human skin. [9]. Therefore, it may be possible to predict skin reactions if we apply the dose-volume histogram or dose-surface histogram relating to the epidermis, dermis, and the subcutaneous tissues also to the human skin.

Please cite this article in press as: Yanagi T et al. Dose-volume histogram and dose-surface histogram analysis for skin reactions to carbon ion radiotherapy for bone and soft tissue sarcoma. Radiother Oncol (2009), doi:10.1016/j.radonc.2009.08.041

What kind of dose-related histogram is suitable for the evaluation of such skin reactions? We tried using two types of histograms in an attempt to answer this question. Firstly, we used the DVH whose ROI was defined as all the organs inside the body covered by the skin at the irradiated area. The reasons for choosing this type of DVH were its ease of preparation with any planning system and the advantages of having a simpler DVH for routine clinical practice. Since this DVH contains the entire volume within the contour, however, the histogram may be influenced by the size of the PTV.

Secondly, we calculated the DSH derived from the skin surface. This calculation was performed based on the hypothesis that the skin surface had the volume of one-pixel-sized-thickness (one pixel: i.e., 0.78–1.26 mm length). According to some reports, attempts for hollow organs have also had satisfactory success with assessing the histogram based on only the outer contour of the organ [10,11]. Since the thickness of the epidermis is 0.15–1.5 mm, this ROI will mainly represent the epidermis.

Other studies have reported the merits of using a band-like region as the ROI, such as a dose–wall histogram, when evaluating the dose of a hollow organ such as the rectum in treating prostate cancer [12]. Since irradiation of subcutaneous tissue affects clinical skin reactions, it may be preferable to use a dose–wall histogram whose ROI includes both the skin and subcutaneous tissue to evaluate the skin reaction. However, as it is not clear over what width range the subcutaneous tissue should be correlated with the development of the skin reaction, it is difficult to adopt an adequate wall width when using a dose–wall histogram. Furthermore, the tumor volume included in the ROI depends largely on how to define the width of the wall. Therefore, a dose–wall histogram is not necessarily adequate for skin evaluation. According to our results, both histograms (DVH/DSH) were correlated with the clinical skin reactions in a certain part of the graph, substantiating the validity of our approach.

There are many reports that discuss skin reactions after X-ray radiotherapy [13,14]. Emami et al. reported a probability of 5% skin necrosis within five years from treatment with 60 Gy for a 30-cm^2 field and 70 Gy for a 10-cm^2 field [13]. Giro et al. reported that high rate of severe radiation dermatitis was observed during radiation therapy with concurrent systemic drug: cetuximab, and they recommended interrupting further treatment if confluent moist desquamation occurs at total doses below 40 Gy [14]. However, carbon ion beams lack the build-up phenomenon, so that the data from X-ray cannot be applied directly to patients treated with carbon ion beams.

Although carbon ion radiotherapy is still in the pioneering stage, many patients have already been treated with fast neutrons, another of the high LET radiation treatment modalities. After treatment with fast neutrons, late damage was greater than that expected on the basis of the early reactions that had been observed [15,16]. This was partly because the relative biological effectiveness (RBE) for late reactions was in general greater than that for acute reactions [17].

The RBE value of carbon ions produced for the therapy at the Institute at Chiba was initially estimated as 3.0 at the distal part of the SOBP (around 8 mm upstream from the distal peak of the SOBP) [6], and we changed the RBE value according to the average LET in the SOBP based on the biological experiments (Fig. 5). Although it was initially well recognized that RBE values changed with fractionation schedule, total dose, and the effect accessed, at the start of the clinical trials in the Institute the RBE was kept constant, even when the fractionation schedule was changed to avoid confusion in clinical trails [6].

In this paper, the institutional protocol was still adopted (GyE = physical dose × RBE), because the study was deeply correlated with practical clinical use. In the future, further clinical observations of the normal tissue reaction after carbon ion radiotherapy might lead to more suitable RBE values for various normal tissues and various fractionation schedules.

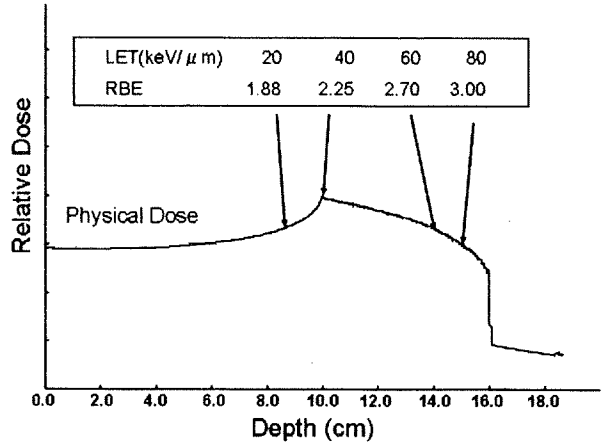

Fig. 5. RBE and LET values used in clinical study (carbon ion, 290 MeV, SOBP = 60 mm). Average LET at the depth was used. The relationship between RBE and LET was obtained from the biological experiments preceded to the commencement of clinical studies [6].

From the results of the present study, all the lesions developing grade 3 or 4 late skin reactions were treated with more than 70.4 GyE as the prescribed dose to the PTV (Table 2). Univariate analysis showed the correlation between the prescribed dose and the late skin reaction (Table 4). It was indicated that severe skin reaction may not develop if the prescribed dose is 64 GyE or less. However, the local control rate of bone and soft tissue sarcomas is dose-dependent. According to Kamada et al., the local control rates of patients receiving 64 GyE or more were significantly better than those of patients with 52.8–57.6 GyE [3], meaning that a higher dose should be used for good local control. Thus, some reliable prognostic parameters are called for.

As shown in Table 3, 3 of the 4 patients who developed grade 4 late skin reactions had the tumor located in the sacrum. The sites of the skin reactions of these patients were at the gluteal fold. This region is notorious for developing decubitus ulcer easily. However, almost all the patients who were treated in the sacral region in this study spent their time in a prone position because of their pain. Thus, these ulcers may be correlated with the irradiation mainly, not mechanical pressure.

It has also been found that the DSH parameter ($S_{60} > 20$ cm^2) was better suited than the DVH parameter ($V_{64} > 100$ ml) for evaluating late skin reactions. This may suggest that skin reactions, even in the late phase, are mainly related to superficial parts of the skin. Recent reports using intensity-modulated radiation therapy (IMRT) suggest that for the sake of avoiding severe skin reactions it might be more effective to plan the PTV a little removed from the skin [18]. In NIRS, we have already obtained successful results with similar methods applied for carbon ion irradiation. Thus, from a clinical point of view, the importance of the superficial parts of the skin in late skin reactions is clearly indicated.

Although no direct relationship was found to exist between the acute and late reactions, the present study showed that a tendency of a relationship does exist between these two reactions for the specific dose fractionation schedule used for this group of patients. With the recent change from conventional radiotherapy to more aggressive schedules, it has been noted that a non-healing-related acute response can directly progress into a late effect. This late effect has been termed "consequential late effect" (CLE) [19]. CLEs are mainly found in those organ systems in which a barrier against mechanical or chemical stress is established by the acutely responding component, such as the urinary and intestinal systems, in mucosa and skin. Bentzen and Overgaard reported, for example,

Please cite this article in press as: Yanagi T et al. Dose–volume histogram and dose–surface histogram analysis for skin reactions to carbon ion radiotherapy for bone and soft tissue sarcoma. Radiother Oncol (2009), doi:10.1016/j.radonc.2009.08.041

based on the data of 229 patients, that patients who developed moist desquamation in the early reaction had a statistically significantly increased risk of developing telangiectasia in the late reaction after X-ray radiotherapy [20]. The observation, at the present study, that most lesions showed the same grade or a 1-grade difference between early and late reactions seemed to support these results. Furthermore, one patient developed consequential ulcer as a consequence of the development of early moist desquamation that is difficult to heal. This case was considered CLE.

Conclusion

Skin was a critical organ in heavy charged particle radiotherapy, with multiple factors contributing to skin reactions. The area irradiated with over 60 GyE (S_{60} > 20 cm^2) on DSH was found to correlate significantly with late skin reactions (≧grade 3).

Acknowledgements

The authors thank Mitsuji Wakaisami, Hiroshi Asakura and Norikazu Tanabe, technologists, for their contribution of the DVH/DSH calculation.

References

[1] Tsujii H, Morita S, Miyamoto T, et al. Preliminary results of phase I/II carbon ion therapy at National Institute of Radiological Sciences. J Brachyther Int 1997;13:1–8.
[2] Tsujii H, Morita S, Miyamoto T, et al. The current status and perspective of heavy-ion therapy. In: Proceedings of the sixth international meeting on progress in radio-oncology, Bologna, Monduzzi Editore S.p.A; 1998. p. 709–21.
[3] Kamada T, Tsujii H, Tsuji H, et al. Efficacy and safety of carbon ion radiotherapy in bone and soft tissue sarcoma. J Clin Oncol 2002;20:4466–71.
[4] Endo M, Koyama-Ito H, Tsujii H, et al. HIPLAN – a heavy ion treatment planning system at HIMAC. J Jpn Soc Ther Radiol Oncol 1996;8:231–8.
[5] International commission on radiation units and measurements. Prescribing, recording, and reporting photon beam therapy (supplement to ICRU Report 50). ICRU Report 62, Bethesda; 1999. p. 3–20.
[6] Kanai T, Endo M, Minohara S, et al. Biophysical characteristics of HIMAC clinical irradiation system for heavy-ion radiation therapy. Int J Radiat Oncol Biol Phys 1999;44:201–10.
[7] Cox JD, Stetz BS, Pajak TF. Toxicity criteria of the Radiation Therapy Oncology Group (RTOG) and the European Organization for Research and Treatment of Cancer (EORTC). Int J Radiat Oncol Biol Phys 1995;31:1341–6.
[8] Hopewell JW. Mechanisms of the action of radiation on skin and underlying tissues. Br J Radiol (Suppl) 1986;19:39–51.
[9] Bentzen SM, Saunders MI, Dische S, et al. Radiotherapy-related early morbidity in head and neck cancer: quantitative clinical radiobiology as deduced from the CHART trial. Radiother Oncol 2001;60:123–35.
[10] Fenwick JD, Khoo VS, Nahum AE, et al. Correlations between dose–surface histograms and the incidence of long-term rectal bleeding following conformal or conventional radiotherapy treatment of prostate cancer. Int J Radiat Oncol Biol Phys 2001;49:473–80.
[11] Meijer GJ, van den Brink M, Hoogeman MS, et al. Dose–wall histograms and normalized dose–surface histograms for the rectum: a new method to analyze the dose distribution over the rectum in conformal radiotherapy. Int J Radiat Oncol Biol Phys 1999;45:1073–80.
[12] Boersma LJ, van den Brink M, Bruce AM, et al. Estimation of the incidence of late bladder and rectum complications after high-dose (70–78 Gy) conformal radiotherapy for prostate cancer using dose–volume histograms. Int J Radiat Oncol Biol Phys 1998;41:83–92.
[13] Emami B, Lyman J, Brown A, et al. Tolerance of normal tissue to therapeutic irradiation. Int J Radiat Oncol Biol Phys 1991;21:109–22.
[14] Giro C, Berger B, Boelke E, et al. High rate of severe radiation dermatitis during radiation therapy with concurrent cetuximab in head and neck cancer: results of a survey in EORTC institute. Radiother Oncol 2009;90:166–71.
[15] Stone RS, Larkin JC. Treatment of cancer with fast neutrons. Radiology 1942;39:608–20.
[16] Duncan W. An evaluation of the results of neutron therapy trials. Acta Oncol 1994;33:299–306.
[17] Hall EJ. Radiobiology for the radiologist. 4th ed. Philadelphia: J.B. Lippincott; 1994. p. 157 and 217.
[18] Lee N, Chuang C, Quivey JM, et al. Skin toxicity due to intensity-modulated radiotherapy for head-and-neck carcinoma. Int J Radiat Oncol Biol Phys 2002;53:630–7.
[19] Doerr W, Hendry JH. Consequential late effects in normal tissues. Radiother Oncol 2001;61:223–31.
[20] Bentzen SM, Overgaard M. Relationship between early and late normal-tissue injury after postmastectomy radiotherapy. Radiother Oncol 1991;20:159–65.

J Gastrointest Surg (2008) 12:1391–1398
DOI 10.1007/s11605-008-0540-9

Interval Period Tumor Progression: Does Delayed Hepatectomy Detect Occult Metastases in Synchronous Colorectal Liver Metastases?

Hiroyuki Yoshidome · Fumio Kimura · Hiroaki Shimizu · Masayuki Ohtsuka · Atsushi Kato · Hideyuki Yoshitomi · Katsunori Furukawa · Noboru Mitsuhashi · Dan Takeuchi · Ayako Iida · Masaru Miyazaki

Received: 12 November 2007 / Accepted: 14 April 2008 / Published online: 20 May 2008

Abstract
Background Rapid remnant liver recurrence in patients with synchronous colorectal liver metastases (CRLM) is occasionally experienced after simultaneous colorectal and liver resection. We evaluated the tumor progression during interval periods to determine whether delayed hepatic resection detects occult metastases.
Methods One hundred thirty-seven patients underwent hepatectomy for synchronous CRLM. Up to 2003, 116 patients underwent simultaneous colorectal and hepatic resection. From 2004 onward, we identified 21 patients undergoing delayed hepatectomy for synchronous CRLM. The tumor progression during interval was determined by a dynamic computed tomography scan.
Results Median/mean interval between the two evaluations prior to the first and second surgery was 2/2.4 months. The median/mean number of metastases detected at each evaluation was 2/3.3 and 3/4.6, respectively. Nine of the 21 (43%) patients had new detectable metastatic lesions after reevaluation. For 11 of the 21 patients, it was necessary to reconsider planned surgical procedure which was determined prior to colorectal surgery. Hepatic disease-free survival was significantly different between patients undergoing delayed and simultaneous hepatectomy. Multivariate analysis showed that the delayed hepatectomy was a significant independent prognostic factor in hepatic disease-free survival.
Conclusion Tumor progression was recognized and occult metastases were detected after the interval reevaluation. Delayed hepatectomy may be a useful approach to reduce rapid remnant liver recurrence in synchronous CRLM.

Keywords Timing of metastases · Occult metastases · Prognostic factors · Liver resection

Abbreviations

CRLM	colorectal liver metastases
CEA	carcinoembryonic antigen
CA19-9	carbohydrate antigen 19-9
CT	computed tomography

H. Yoshidome · F. Kimura · H. Shimizu · M. Ohtsuka · A. Kato · H. Yoshitomi · K. Furukawa · N. Mitsuhashi · D. Takeuchi · A. Iida · M. Miyazaki (✉)
Department of General Surgery,
Chiba University Graduate School of Medicine,
1-8-1 Inohana, Chuo-Ku,
Chiba 260-0856, Japan
e-mail: masaru@faculty.chiba-u.jp

Introduction

Hepatic resection for colorectal liver metastases (CRLM) is the only potentially curative option, and the 5-year survival rate has been reported to range between 26% and 45%.[1–5] Previous studies have shown that there are several prognostic factors, such as the timing of metastases, the number of nodules, tumor size, a higher stage of primary cancer, extrahepatic metastases, and hepatoduodenal lymph node involvement.[2,5,6–14] Approximately 60% of the patients undergoing hepatic resection for CRLM experienced disease recurrence.[2] While aggressive surgery can prolong survival even in patients with synchronous and multiple CRLM, rapid remnant liver recurrence is occasionally experienced in patients with synchronous CRLM after simultaneous colorectal and hepatic resection. Patients with rapid remnant liver

recurrence may gain no survival benefit from hepatectomy, which may be one reason of their survival being worse than that of patients with metachronous CRLM. Thus, the most appropriate timing for hepatic resection for synchronous CRLM remains to be determined.

Previous studies demonstrated that the survival benefit of hepatic resection is determined by the biological features of the tumor.[10] Scheele et al. demonstrated that the micrometastases are likely to remain unresected in the remnant liver in patients undergoing synchronous surgery.[9] This suggests that the interval hepatic resection is a possible means of assessing tumor biological features for the identification of occult metastases. The only previous study of which we are aware, by Elias, reported only a 5% to 10% chance of new metastases being detected during the interval between separate operations (3–6 months).[15] However, preoperative radiological techniques such as multidetector row computed tomography (CT) have recently been developed and could define the extent of metastases more accurately.[16] Overall, the biological features of tumors, including tumor progression and the effect of interval resection on survival, have not been well-defined in patients with synchronous CRLM. In the present study, we reviewed our cases of patients who had undergone hepatic resection for CRLM to examine the changes in metastatic lesions during the interval period and to determine whether the delayed hepatic resection reduces the hepatic recurrence in patients with synchronous CRLM.

Materials and Methods

Patients

Between March 1985 and December 2006, a total of 137 patients underwent initial liver resection for synchronous CRLM in our institution. The medical records of these patients were retrospectively reviewed. In this study, synchronous metastases were defined as metastases diagnosed before colorectal surgery or at the time of surgery. Up to 2003, 116 patients with synchronous CRLM underwent simultaneous colorectal and hepatic resection. We previously reported that the synchronous metastasis is a significant factor by univariate analysis but is not independently significant prognostic factor by multivariate analysis.[4] However, the timing of metastases (synchronous) has become an independent significant prognostic factor defined by the multivariate analysis.[17] We also previously reported that 31% of the patients who underwent hepatectomy for CRLM had micrometastases that had not been detected.[4] Thus, we hypothesized that the rapid remnant liver recurrences in synchronous CRLM may originate from the occult hepatic metastases that cannot be detected at the time of hepatic resection. Therefore, from 2004 onward, our strategy for the treatment of synchronous liver metastases has been changed to perform separate operations for primary cancer and CRLM. From 2004 onward, 21 consecutive patients with synchronous CRLM underwent separate colorectal and hepatic resection.

Preoperative Evaluation

All patients were preoperatively evaluated by colonoscopy, abdominal ultrasonography, and thoracoabdominal enhanced CT. Identical thoracoabdominal-enhanced CT was performed for reevaluation prior to the delayed hepatectomy in patients undergoing delayed hepatectomy. In this study, hepatic metastasis was defined by an abdominal CT scan. Multidetector row CT has been used for the evaluation from 2002 onward. Remnant liver functional reserve was predicted from the indocyanine green retention rate at 15 min. Hepatectomy was performed regardless of the number of tumors whenever a remnant functional hepatic reserve was predicted to be preserved. Future remnant liver volume was predicted by CT volumetry in every patient from 1998 onward. Patients with a predicted remnant liver volume $\geq$35% of the total liver volume underwent liver resection without preoperative portal vein embolization from 1998 onward. The hepatectomy procedure did not differ whether the patients underwent simultaneous or delayed hepatectomy. With reference to synchronous extrahepatic metastases, patients with resectable pulmonary metastases at the time of diagnosis of liver metastases were surgical candidates. Based on this decision-making, three patients in the interval resection group underwent irinotecan-based chemotherapy (CPT-11+S-1) because they were diagnosed as irresectable at the time of reevaluation after colorectal surgery. Sixty-eight of the 116 patients in the simultaneous resection group received either hepatic arterial or systemic (oral) 5-fluorouracil-based chemotherapy. Twelve of the 21 patients in the interval resection group received systemic oral 5-fluorouracil-based chemotherapy.

Follow-up

After hepatic resection, all patients were followed up. Tumor markers such as carcinoembryonic antigen and carbohydrate antigen 19-9 were determined every 3 months. Ultrasonography, thoracoabdominal CT, or total colonoscopy was performed to examine recurrence. Patients were followed for survival until death or October 1, 2007.

Statistical Analysis

Data were expressed as median/mean, and variables were analyzed using the Mann–Whitney U test, Fisher's exact test, or chi-square test as appropriate. Hepatic disease-free

survival was calculated by the Kaplan–Meier method, and comparisons were performed using the log-rank test. Multivariate analysis was performed using the Cox proportional hazards model. We analyzed survival on an intention-to-treat basis. For all evaluations, a p value <0.05 was considered significant.

Results

Patient Characteristics

A total of 137 patients with synchronous CRLM who underwent hepatic resection were identified, of whom 83 were men and 54 were women. Up to 2003, 116 patients with synchronous CRLM underwent simultaneous colorectal and hepatic resection. Twenty-one consecutive patients with synchronous CRLM underwent delayed hepatic resection from 2004 onward. Median age was 66 years old (range, 41–75 years old). Twelve were men and nine were women.

Reevaluation of Tumor Progression during Interval Periods

The primary tumor was T3 or T4 in 21 patients and there were lymph node metastases in 15 of the 21 (71%). The median/mean duration of each evaluation by CT scan which was performed prior to the first (primary tumor resection) and second (hepatic resection) operations was 2/2.4 months (Table 1). The median/mean number of metastases was increased after reevaluation (from 2/3.3 to 3/4.6; Table 1). Nine of the 21 (43%) patients had new detectable metastatic lesions in different segments defined by Couinaud's classification after reevaluation, and eight patients had new metastases in the future remnant liver as determined by hepatectomy procedure which had been planned prior to primary colorectal tumor resection (Table 2). One patient (case 16), who had major complications associated with primary surgery, showed a significant increase in the number of metastases after reevaluation (Table 2). Unilateral metastases became bilateral in two patients. For 11 of the 21 patients, it was necessary to reconsider the planned surgical procedure of hepatectomy which was determined before colorectal surgery. At reevaluation after primary colorectal surgery, 3 patients underwent preoperative irinotecan-based chemotherapy (CPT-11+S-1) because they were diagnosed as irresectable as a result of a lack of liver volume due to the increased numbers of multiple bilateral metastases in one, an ill-located huge tumor in another, and an extrahepatic disease defined prior to colorectal resection (bilateral multiple lung metastases) in the third. All of the three patients underwent curative hepatic resection after chemotherapeutic downstaging. Two patients underwent preoperative portal vein embolization because of a lack of hepatic volume.

Table 1 Characteristics of Metastatic Lesion before or after Colorectal Resection (n=21)

Category	Resection of primary carcinoma	Number of cases	
		Before	After
Maximum diameter	median/mean (mm)	29.8/32.8	34.8/43.8
5 cm or less		19	17
More than 5 cm		2	4
Number of tumors	median/mean	2/3.3	3/4.6
Solitary		5	4
2–3 nodules		9	8
4 or more		7	9
Location			
Unilateral		8	6
Bilateral		13	15
Extrahepatic metastasis			
Lung		1	1

Survival and Prognostic Factors in Synchronous Metastases

To determine whether interval reevaluation identified a subgroup of patients with improved prospects of survival, the hepatic disease-free survival of all 21 patients undergoing delayed hepatic resection was compared with that of all the 116 patients undergoing simultaneous colorectal and hepatic resection. Patient characteristics are shown in Table 3. Forty-eight percent of patients who underwent simultaneous resection for synchronous CRLM had hepatic recurrence within 12 months (Fig. 1) and 61% of patients had recurrence within 24 months. To identify a subset of patients who could undergo either simultaneous or interval hepatic resection, we examined tumor-related factors. In patients who underwent simultaneous hepatic resection, multiple liver metastases and positive nodal involvement of the primary colorectal cancer were significant factors indicative of early recurrence within 12 months after hepatectomy (Table 4). Multiple liver metastases were a significant factor in early recurrence within 24 months after hepatectomy (data not shown). However, there was no significant predictive factor for interval recurrence in patients who underwent interval hepatic resection (Table 4). Hepatic disease-free survival was significantly different between the patients undergoing delayed hepatic resection (n=21) and simultaneous hepatic resection (n=116) based on an intention-to-treat analysis (p=0.0028; Fig. 1a). Hepatic recurrence within 12 months after hepatectomy was reduced in the delayed resection group (13%) compared with the simultaneous resection group. We examined hepatic disease-free survival in subgroups strat-

Table 2 Tumor Progression during Interval Period (n=21)

No.	Age	Sex	Tumor location (before)	Tumor location (after)
1	63	F	S5 (1), S6 (3), S7 (1), S8 (2)	S5 (1), S6 (3), S7 (1), S8 (2)
2	63	F	S3 (2), S6 (3), S7 (1), S8 (3)	S3 (2), **S4 (2)**, **S5 (2)**, S6 (3), S7 (1), S8 (3)
3	70	M	S3 (1), S6 (1), S8 (1)	S3 (1), **S4 (2)**, S6 (1), **S8 (2)**
4	74	F	S8 (1)	S (1)
5	65	F	S4 (2), S7 (1), S8 (1)	S4 (2), S7 (1), S8 (1)
6	70	F	S1 (1), S4 (1), S6 (1), S7 (1), S8 (1)	S1 (1), S4 (1), S6 (1), S7 (1), S8 (1)
7	70	M	S4 (1), S5 (1), S6 (1), S8 (1)	S4 (1), S5 (1), **S6 (2)**, S8 (1)
8	66	M	S4-5 (1), S6 (1), S7 (2)	**S2 (1)**, S4–5 (1), S6 (1), S7 (2), **S8 (1)**
9	41	F	S3 (1), S8 (1)	S3 (1), **S4 (1)**, **S4–8 (1)**, S8 (1)
10	71	M	S4 (1), S5 (1)	S4 (1), S5 (1)
11	73	F	S7 (1)	S7 (1), **S4 (1)**, **S6 (1)**
12	61	M	S2 (1), S4 (1)	S2 (1), S4 (1)
13	75	M	S6 (1), S7 (1)	S6 (1), S7 (1), **S4 (1)**
14	67	M	S3 (1), S8 (1)	S3 (1), S8 (1)
15	75	F	S2 (1), S3 (1), S6 (1)	S2 (1), S3 (1), S6 (1)
16	50	M	S1 (1), S2 (2), S4 (2), S6 (2), S7 (1), S8 (1)	S1 (1), S2 (2), **S3 (1)**, S4 (2), **S5 (2)**, S6 (2), **S7 (3)**, **S8 (3)**
17	67	M	S5 (1)	S5 (1)
18	61	M	S2, 3, 4, 5, 8 (1)	S2, 3, 4, 5, 8 (1)
19	58	F	S3 (1)	S3 (1)
20	46	M	S3 (1), S5 (1), S6 (1), S7 (2)	S3 (1), **S5 (2)**, **S6 (2)**, S7 (2), **S8 (1)**
21	50	M	S4 (2)	S4 (2)

Number of metastases is shown in parenthesis. A new metastatic lesion is indicated by bold characters and a new lesion appeared in different segments is underlined.
S Segment (defined by Couinaud's classification)

ified by the number of metastases (solitary/multiple). Hepatic disease-free survival was significantly different between patients undergoing delayed hepatic resection (n=17) and simultaneous hepatic resection (n=75) in multiple CRLM (p=0.0014; Fig. 1b). Hepatic disease-free survival was not significantly different between patients undergoing delayed hepatic resection (n=4) and simultaneous hepatic resection (n=41) in solitary CRLM (p=0.2767; Fig. 1c),

Table 3 Characteristics of Patients who Underwent Interval Hepatic Resection (n=21) or Synchronous Resection (n=116)

Category	Interval (n=21)	Synchronous (n=116)	p value
Sex			
Man	12	71	0.914
Woman	9	45	
Primary site			
Colon	11	67	0.827
Rectum	10	49	
Histology (primary)			
Well	4	31	0.092
Moderately	13	81	
Poorly, mucinous	3	4	
Primary tumor			
T1	0	2	0.645
T2	0	6	
T3	11	61	
T4	10	47	
Regional lymph nodes			
Negative	6	34	0.848
Positive	15	82	
Number of metastatic nodules			
Solitary	4	41	0.226
Multiple	17	75	

T factor is defined by TNM classification.

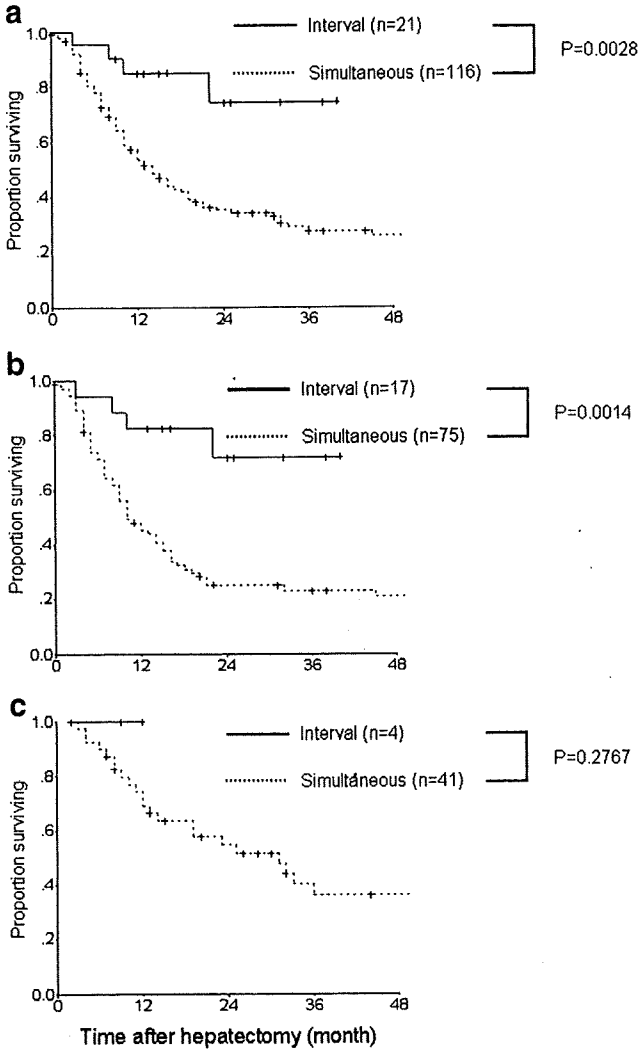

Figure 1 Hepatic disease-free survival of patients after hepatectomy was calculated by the Kaplan–Meier method. **a** Patients with synchronous colorectal liver metastases were divided into simultaneous hepatectomy (n=116) and interval hepatectomy (n=21) groups. **b** Patients with synchronous and multiple colorectal liver metastases were divided into simultaneous hepatectomy (n=75) and interval hepatectomy (n=17) groups. **c** Patients with synchronous and solitary colorectal liver metastases were divided into simultaneous hepatectomy (n=41) and interval hepatectomy (n=4) groups. A comparison was performed using the log-rank test. A p value <0.05 was considered significant.

although the number of patients in delayed hepatic resection was small. Interval resection was demonstrated by multivariate analysis to be a significant independent prognostic factor in hepatic disease-free survival in patients with synchronous CRLM (Table 5).

Discussion

The indication of hepatectomy for CRLM has recently been extended to include patients with multiple bilobar metastases, synchronous pulmonary metastases, and the invasion of major vasculatures.[18–20] The timing of metastases was reported to be a significant prognostic factor for survival.[9] Our previous report indicated that the timing of metastases was not a statistically significant independent prognostic factor, although more recently, it has become so.[4,17] One reason for this may be that the patients with more advanced synchronous CRLM have become candidates for hepatic resection. The other reason for this may be that the synchronous CRLM are likely to include occult micrometastases which cannot be detected preoperatively. We previously reported that 31% of the patients who underwent hepatectomy for CRLM had micrometastases,[4] and Yokoyama et al. showed that micrometastases are detectable by immunohistochemistry in 68% of the resected specimens and suggested that the micrometastases may be associated with a intrahepatic recurrence.[21]

Table 4 Association between Tumor (Primary and Metastatic)-Related Factors and Early Recurrence (within 12 months after Hepatectomy) in Simultaneous Resection Group (n=116) or Tumor Progression during Interval in Interval Resection Group (n=21)

Category	Recurrence (yes)	Recurrence (no)	p value
Within 12 months after simultaneous hepatectomy (n=116)	n=56	n=60	
Primary site			
Colon	35	32	0.418
Rectum	21	28	
Regional lymph nodes			
Negative	45	37	0.045
Positive	11	23	
Number of metastatic nodules			
Solitary	14	27	0.032
Multiple	42	33	
Tumor			
More than 5 cm	20	15	0.292
5 cm or less	36	45	
Iinterval recurrence in delayed hepatectomy (n=21)	n=9	n=12	
Primary site			
Colon	5	6	1.000
Rectum	4	6	
Regional lymph nodes			
Negative	2	4	0.659
Positive	7	8	
Number of metastatic nodules			
Solitary	1	5	0.178
Multiple	8	7	
Tumor size			
More than 5 cm	0	2	0.486
5 cm or less	9	10	